Simulation of the energy level scheme of Nd^{3+} and Eu^{3+} ions in rare-earth orthovanadates and phosphates

1991 J. Phys.: Condens. Matter 3 6829

(http://iopscience.iop.org/0953-8984/3/35/012)

J. Phys.: Condens. Matter 3 (1991) 6829–6843. Printed in the UK

Simulation of the energy level scheme of Nd^{3+} and Eu^{3+} ions in rare-earth orthovanadates and phosphates

Elisabeth Antic-Fidancev†, Jorma Hölsä‡, Michelle Lemaitre-Blaise† and Pierre Porcher†

† Laboratoire des Elements de Transition dans les Solides, UPR, 210 CNRS, 1, place A. Briand, F-92195 Meudon, France

‡ Department of Chemical Engineering, Helsinki University of Technology, SF-02150 Espoo, Finland

Received 12 April 1991

Abstract. The absorption spectra of the Nd^{3+} ion in the tetragonal xenotime-type $NdVO_4$ and in the monoclinic monazite-type $LaVO_4$, $LaPO_4$ and $NdPO_4$ as well as the luminescence of the Eu^{3+} ion in $LaVO_4$ and $LaPO_4$ were measured and the spectra were analysed according to the appropriate symmetry of the RE site. In addition to pure zero-phonon electronic lines the absorption spectra of the Nd^{3+} ion showed extensive vibronic side bands which were identified with the aid of the measured Raman scattering spectra of $LaVO_4$:Nd^{3+} and $NdVO_4$. Based on the energy level schemes derived from the absorption and luminescence spectra the parametrization of the free-ion and crystal-field effects were carried out with good results as indicated by the low RMS deviation values. The parameter sets for Nd^{3+} and Eu^{3+} ions in the same matrices are consistent with each other but no correlation was found between sets for matrices of different structures.

1. Introduction

The trivalent RE^{3+} ions offer a very convenient and reliable tool for chemists and physicists to study the different electronic and magnetic interactions and their magnitude in solid state. This, of course, is due to the position of $4f^N$ electrons well shielded from the effect of the neighbouring ions. The shielding results in discrete and well defined energy level schemes as well as in usually rather weak coupling between the electronic and vibrational wave functions. One of the most popular RE^{3+} ions used as a spectroscopist's tool is Nd^{3+} with the $4f^3$-electron configuration which, at the same time, offers both the maximum amount of interactions to be studied and still a rather simple and conveniently calculable set of energy levels with only 182 Kramers' levels. Accordingly, the investigations based on the energy level scheme of the Nd^{3+} ion in different matrices can be found relatively frequently in the literature. At least the following matrices have been studied in considerable detail: LaF_3 [1, 2], NdF_3 [3], $LaCl_3$ [4, 5], $NdCl_3$ [6], $LaBr_3$ [7], $Cs_2NaRECl_6$ [8–10], $LiYF_4$ [11, 12], KY_3F_{10} [13], $CsCdBr_3$ [14], Nd_2O_3 [15], Y_2O_3 [16], NdOCl [17], $NdAlO_3$ [18], $YAlO_3$ [19, 20], Nd_2O_2S [21], Nd_2S_3 [22], RE_2BaZnO_5 [23], different garnets [24–26], $REPO_4$ [27, 28] and $REVO_4$ [29, 30], $Nd(EtSO_4)_3{\cdot}9H_2O$ [31, 32], $Na_3[Nd(oxydiacetate)_3]{\cdot}2NaClO_4{\cdot}6H_2O$ [33], $CaWO_4$ [34], $PbWO_4$ [35] and $PbMoO_4$ [36].

0953-8984/91/356829 + 15 $03.50

The optical properties of several RE^{3+} ions in $REVO_4$ and $REPO_4$ matrices have also been studied, i.e. Eu^{3+} in YVO_4 [37–41] and in $LuVO_4$ [41], Ho^{3+} in YPO_4 [27], Er^{3+} in YVO_4 [29, 42–43] and in YPO_4 [29, 42] and finally Tm^{3+} in YVO_4 [44, 45] and in YPO_4 [27]. However, these investigations have been concentrated on the xenotime-type structure for the obvious reason that this structure has much higher point symmetry of the RE site, D_{2d}, than the monazite structure, C_1.

Since the lower-symmetry monazite structure has so far been omitted, our aim was to carry out the study of the energy level schemes in the Nd^{3+} ion in the $NdVO_4$–$LaVO_4$ system and to compare the results with that obtained for $NdPO_4$. The ^7F_J level scheme of the Eu^{3+} ion in the $LaVO_4$ and $LaPO_4$ matrices was also investigated for comparison.

2. Experimental details

2.1. Sample preparation

The $REVO_4$ and $REPO_4$ powder samples were prepared from a solid state reaction between corresponding RE sesquioxides and ammonium vanadate or phosphate. The said mixtures were first heated at 500 °C for 3 h, then at 700 °C for 2 h and finally at 1050 °C for 15 h. The routine x-ray powder diffraction analysis of the products revealed only the presence of orthovanadate or orthophosphate phases. For luminescence measurements the $LaVO_4$:Eu^{3+} and $LaPO_4$:Eu^{3+} powder samples were doped with a small amount of the trivalent europium ion (about 1 and 5 mol% of the total RE amount) replacing the host cation. The random and uniform substitution was ensured because of the small solubility differences between RE^{3+} ions. The Nd^{3+} content in $LaVO_4$ was much higher, close to 15 mol%, as required by the absorption measurements.

2.2. Optical measurements: absorption and luminescence

The absorption spectra of pure $NdVO_4$, pure $NdPO_4$ and doped $LaVO_4$:Nd^{3+} were obtained with a 3.4 m Jarrell–Ash grating spectrograph using photographic detection. All absorption measurements were carried out at 300, 77 and 4.2 K between 325 and 950 nm (10 500 and 30 000 cm^{-1}). Higher energies could not be reached owing to the matrix (MO_4^{3-}) absorption.

The luminescence spectra of $LaVO_4$:Eu^{3+} and $LaPO_4$:Eu^{3+} powder samples were detected under UV excitation at 300 and 77 K. The radiation from a 200 W mercury lamp was centred with wide-band filters below 300 nm to correspond to the strongly absorbing MO_4^{3-} band of the host matrix. The energy transfer from the MO_4^{3-} group to Eu^{3+} ion resulted in emission from the latter species which was detected with a 1 m Jarrell–Ash monochromator and a Hamamatsu R374 photomultiplier. The luminescence was recorded in the wavelength range between 575 and 750 nm.

2.3. Optical measurements: Raman scattering

The room temperature Raman scattering spectra of $REMO_4$ powder samples were obtained with Spectra Physics 164 argon ion laser excitation. The scattered radiation was dispersed with a Jobin–Yvon T800 triple monochromator and detected with a Hamamatsu R464 photomultiplier. The resolution of the equipment after the photon counting and electronic treatment was better than 3 cm^{-1}. The infrared absorption spectra for $REVO_4$ and $REPO_4$ were taken from [46, 47].

2.4. Crystal structure of $REVO_4$ and $REPO_4$

The crystal structures of $REVO_4$ (RE ≡ Ce–Lu and Y) corresponding to the well known RE mineral xenotime are isomorphous belonging to the tetragonal crystal system with $I4_1/amd$ (D^{19}_{4h}) (No 141; $Z = 4$) as the space group [48]. The RE orthophosphates yield a similar structure except that the xenotime structure is stable from Gd to Lu (including Y) in the RE series [49]. The RE cation is coordinated to eight oxygen atoms in an arrangement of two interpenetrating tetrahedra yielding D_{2d} as the point symmetry of the single RE site. $LaVO_4$ and lighter members of the orthophosphate series possess the monoclinic monazite-type structure with $P2_1/n$ (C^5_{2h}) (No 14; $Z = 4$) as the space group [49]. In this structure the RE site is of much lower symmetry, C_1, than in the xenotime version. The RE coordination to nine oxygen atoms is very distorted but can be characterized best as a tricapped trigonal prism.

2.5. Theoretical treatment of experimental data

The major interactions resulting in the free-ion electron structure of the RE^{3+} ions with the $4f^N$ configuration include the electrostatic repulsion between the 4f electrons and the coupling of their spin and orbital angular momenta. Several minor contributions within the free-ion scheme can be taken into account in addition to the crystal-field effect. A rather recent review [1] can be used to furnish further details about the subject. The Hamiltonian used in this study was as follows:

$$H = H_0 - \sum_{k=0,1,2,3} E^k(nf, nf)e_k + \zeta_f A_{SO} + \alpha L(L+1) + \beta G(G_2) + \gamma G(R_7) + \sum_{k=2,3,4,6,7,8} T^k t_k + H_{cf} \quad (1)$$

where H_0 is the spherically symmetric one-electron part of the free-ion Hamiltonian, E^k and ζ_f are the electrostatic and spin–orbit integrals; e_k and A_{SO} represent the angular parts of the interactions mentioned above. For configurations of two or more equivalent electrons the two-body interactions can be taken into consideration. The appropriate two-body correction terms include α, β and γ; L is the total orbital angular momentum; $G(G_2)$ and $G(R_7)$ are the Casimir operators for the groups G_2 and R_7, respectively. For the $4f^N$-electron configurations with $N > 2$, one can apply the three-body configuration interaction terms which are usually parametrized with the Judd parameters T^k (k = 2, 3, 4, 6, 7 and 8). The t_k are operators transforming according to the irreducible groups G_2 and R_7.

The standard one-electron crystal-field Hamiltonian H_{cf} comprises a sum of the products between the real and imaginary even-rank crystal-field parameters B^k_q and S^k_q and the spherical harmonics C^k_q as follows:

$$H_{cf} = \sum_{kq} [B^k_q(C^k_q + C^k_{-q}) + iS^k_q(C^k_q - C^k_{-q})]. \quad (2)$$

The crystal-field parameters are appropriate to the site symmetry of the RE^{3+} ion in each matrix. Accordingly, for the xenotime structure with D_{2d} as the point symmetry of the RE^{3+} site there exist only five non-zero B^k_q parameters; B^2_0, B^4_0, B^4_4, B^6_0 and B^6_4. On the contrary, there are 27 different real and imaginary crystal-field parameters for the C_1 site symmetry prevailing in the monazite-type $REMO_4$. Such a number of parameters is not realistic for practical purposes and thus the simulation of the Eu^{3+} energy level

scheme was carried out according to the C_{2v} symmetry with nine real B_q^k ($k = 0, 2, 4$ and $6; q \leq k$) crystal-field parameters. As a whole the $4f^3$-electron configuration of the Nd^{3+} ion consists of 182 energy levels and thus the corresponding Hamiltonian involves a symmetric square matrix of size 182 × 182 which can be treated with relative ease on a memory-extended PC without truncation of the basis set of levels.

The $4f^6$ configuration of the Eu^{3+} ion has a total of 3003 $|\alpha SLJM\rangle$ Stark sublevels. Since the treatment of the $4f^6$ configuration as a whole is impractical, some kind of truncation of the wavefunctions is usually introduced. The most simple case is to take into account only the 49 components of the $^7F_{0-6}$ ground multiplet. Such a rather drastic truncation naturally neglects many minor perturbations on the ^7F_J wavefunctions. However, in most cases studied, this restricted set of ^7F_J wavefunctions has been found sufficient to describe in an adequate way the effect of the neighbouring atoms on the electronic structure of the Eu^{3+} ion. The success encountered originates from two facts: first, the ^7F_J ground multiplet is energetically well separated (nearly 12 000 cm^{-1}) from the next highest excited multiplet ($^5D_{0-4}$) and, secondly, the crystal-field operator mixes only wavefunctions with the same multiplicity (the ^7F septet is the only one of that multiplicity within the $4f^6$ configuration).

The actual fitting procedure between experimental and calculated energy level values was conducted with standard least-squares calculations using the σ-value (as defined in equation (3)) as a figure of merit describing the quality of the fit:

$$\sigma = \left(\sum \frac{(E_{exp} - E_{calc})^2}{N_{lev} - N_{par}}\right)^{1/2}. \tag{3}$$

3. Results and discussion

3.1. Raman spectra of $LaVO_4$ and $NdVO_4$

The Raman spectra of $LaVO_4$ and $NdVO_4$ (figure 1) show two regions with several well resolved lines; first, the high-energy region between 745 and 880 cm^{-1} and, secondly, the vibrations below 475 cm^{-1} (table 1). The high-frequency region corresponds to the 'internal' vibrations of the ideally tetrahedral VO_4 group. However, owing to the relatively high number of lines it is evident that the VO_4 groups are distorted, thus lifting the original selection rules and, at the same time, inducing the splitting of the degenerate vibrational levels for the T_d symmetry. The results are in agreement with previous structural data [48].

The second group of lines in the Raman spectra originates mainly from the RE-oxygen vibrations. For the $LaVO_4$ matrix the great number of the peaks is in accordance with the relatively high coordination number of the lanthanum (9) and the low symmetry of the RE site (C_1) which both contribute to the complicated vibrational spectra. A comparison of our results with the corresponding IR data [46, 47] gives good agreement (table 1). Despite the evident general similarity of the Raman spectra of the two vanadates, $LaVO_4$ and $NdVO_4$, the fine structures are substantially different, in accordance with the structural data. In particular in $LaVO_4$ the number of peaks is higher, well in line with its structure of lower symmetry.

3.2. Absorption spectra of Nd^{3+} ion in $NdVO_4$, $LaVO_4$ and $NdPO_4$

The absorption spectra of the Nd^{3+} ion in the $NdVO_4$, $LaVO_4$ and $NdPO_4$ matrices were measured in the wavelength region between 900 and 325 nm (11 000 and 30 500 cm^{-1}).

Table 1. Infrared and Raman spectra of $LaVO_4$ and $NdVO_4$.

ν (cm^{-1})						
$LaVO_4:Eu^{3+}$	$LaVO_4:Nd^{3+}$		$LaVO_4$	$NdVO_4$		
IR	IR	Raman	Raman [46]	IR	Raman	Raman [47]
860	870	880			868	
846	853	860	860 ν_1	860		862 ν_1
830	838	841	844 ν_3			
814	823	819	820 ν_3	815		
800					805	
778	778	793	796 ν_3			799 ν_3
768		788	791 ν_3		790	786 ν_3
745	755	767	771 ν_3	755		
475	483			451	471	468 ν_4
435	440	439	440			
		423	425			
389	398	398	399		380	
360	369	375	376		375	377 ν_2
		352	351			
		330	324			
300	300	307	309			
285				290		
278		252			262	
245		236			235	
230						
211						
207		207				
		188				
		158			151	
		144				
		138				
		125			122	
		112			112	
		103				
		88				
		69				
		63				
		38			37	

At higher energies the strong matrix absorption, i.e. absorption of VO_4^{3-} and PO_4^{3-} groups, overlapped with the 4f–4f transitions of the Nd^{3+} ion, thus preventing the determination of high-energy part of the spectra. In each host matrix the Nd^{3+} ion seems to occupy a single site in accordance with the structure. This fact is confirmed by the absorption at liquid-helium temperature from the lowest crystal-field component of the $^4I_{9/2}$ ground state to the well isolated $^2P_{1/2}$ level which is not split under the effect of the crystal field. This absorption yields only one line for each matrix. In the $LaVO_4$ matrix the upper limit of the Nd^{3+} concentration is about 10 mol%, above which concentration one could also observe the absorption lines originating from the tetragonal $NdVO_4$ form.

The pure electronic zero-phonon lines in the absorption spectra of the Nd^{3+} ion in the $NdVO_4$, $LaVO_4$ or $NdPO_4$ matrices are accompanied by vibronic replica. However,

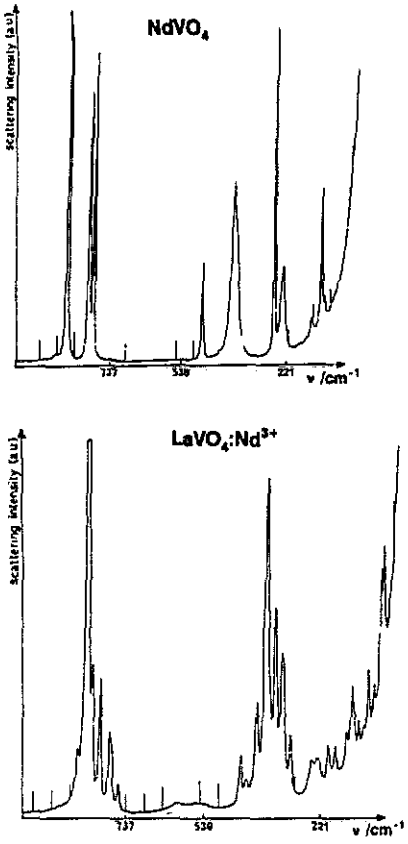

Figure 1. The Raman scattering spectrum of $NdVO_4$ and $LaVO_4$:Nd^{3+}.

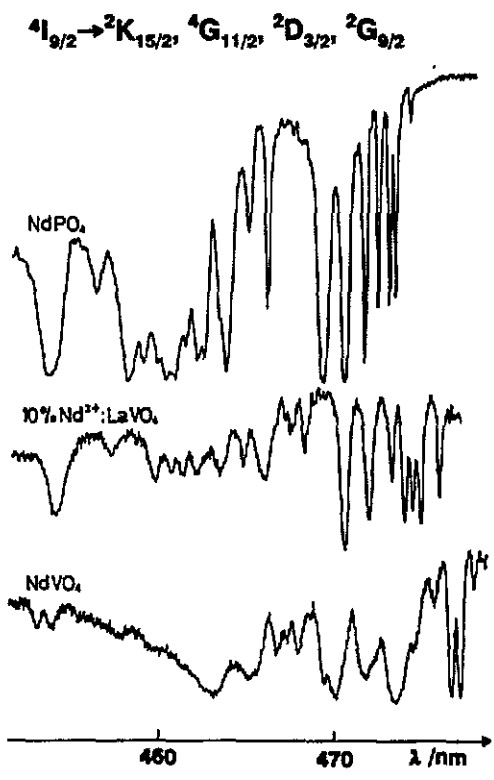

Figure 2. Part of the absorption spectra of the Nd^{3+} ion in $NdPO_4$, $LaVO_4$ and $NdVO_4$ at liquid-helium temperature.

not all transitions are poisoned by the vibronic side bands; the transitions following the selection $\Delta J \leqslant 2$ are most badly affected. The intensity of transitions obeying this selection rule show frequently extensive dependence of the environment of the RE^{3+} ion and are thus called 'hypersensitive' transitions. The hypersensitivity has been subject to extensive discussion in literature and the connection between the presence of vibronic transitions and hypersensitivity has been discussed in detail elsewhere also for the $REVO_4$ system [50, 51]. In our case the presence of strong coupling between the electronic and vibronic levels was considered a nuisance. The part of the absorption spectra of the Nd^{3+} ion in the three matrices shown in figure 2 reveals the basic similarity between the $NdPO_4$ and $LaVO_4$:Nd^{3+} spectra, differing substantially from that of $NdVO_4$.

3.3. Free-ion and crystal-field simulation of the Nd^{3+} energy level schemes

Despite the extensive vibronic structure of the electronic spectra of the Nd^{3+} ion in all matrices studied, the $4f^3$ energy level schemes could be successfully determined (table 2). Up to 90 levels of the 182 allowed Stark levels for the $4f^3$-electron configuration could be detected. The results of the simulation of the free-ion and crystal-field effects in this

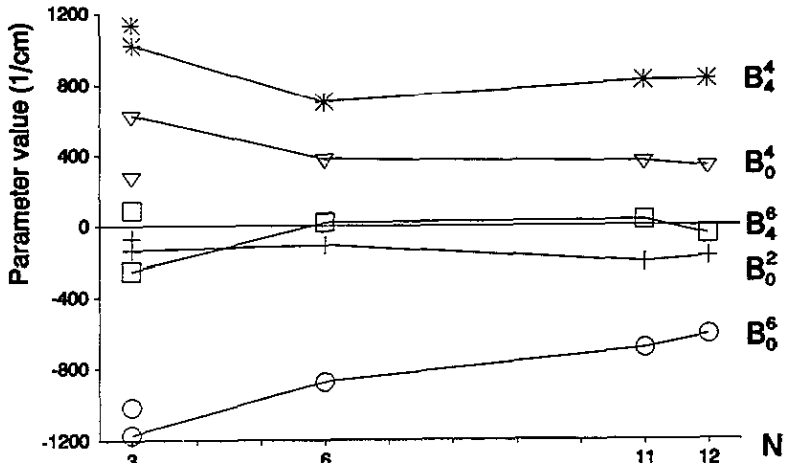

Figure 3. The crystal-field parameter values for $NdVO_4$ and YVO_4:RE^{3+} (RE ≡ Nd, Eu, Er and Tm; i.e. $4f^3$, $4f^6$, $4f^{11}$ and $4f^{12}$ configurations) series.

basis set are given in table 3. At once it can be observed that the simulation could reproduce the experimental energy level scheme in a completely satisfactory way; the RMS deviations have assumed low values (table 3) and no large individual discrepancies occur between the calculated and experimental energy values (table 2). During the simulation it was found that some of the free-ion parameters could not be varied freely owing to the lack of the most determining energy level values. Accordingly, the values of a few parameters were fixed to their customary values.

The free-ion parameter values in table 3 show no considerable variation as a function of the crystal structure of the host or the host cation. However, it is rather surprising to observe an increase in the values of the Racah parameters E^i with increasing size of the host cation, i.e. Nd^{3+} versus La^{3+} in the $REVO_4$ series. Since the E^i-parameters describe the electrostatic interaction between the 4f electrons, their values should be expected to increase with decreasing space for the electrons to reside. A slight trend of this kind can be observed between $LaVO_4$ and $NdPO_4$ but probably the different structure of $NdVO_4$ from $LaVO_4$ hides this trend in the $REVO_4$ series.

In contrast with the similarity of the free-ion parameters irrespective of the crystal structure of the host the crystal-field parameter values for $NdVO_4$ and $LaVO_4$ are completely different. The effect of the different structures can be seen not only in the different number of the crystal-field parameters but also in their dissimilar values. On the other hand, the structural similarity between $LaVO_4$ and $NdPO_4$ results also in rather similar crystal-field parameter values. A comparison with the crystal-field parameter values for other closely related systems, i.e. YVO_4:RE^{3+} [29, 37, 40, 45] shows the previous results consistent with our values for $NdVO_4$ as revealed by figure 3. In fact, despite the different matrix the evolution of the B_q^k-parameter values is rather smooth through the whole RE series. The crystal-field effect should in theory increase towards the end of the RE series owing to the increased nuclear charge. However, even the reverse trend can be observed in the YVO_4:RE^{3+} series. This may be due to the fact that, when the smaller Er^{3+} and Tm^{3+} ($4f^{11}$ and $4f^{12}$ configurations, respectively) replace the Y^{3+} matrix cation, the space available in fact expands instead of shrinking. The

Table 2. Experimental and calculated energy levels of the Nd^{3+} ion in $NdVO_4$, $LaVO_4$ and $NdPO_4$.

	Energy level (cm^{-1})					
	$NdVO_4$		$LaVO_4:Nd^{3+}$		$NdPO_4$	
	Calculated	Experimental	Calculated	Experimental	Calculated	Experimental
$^4I_{9/2}$	−11	0	3	0	22	0
	124	106	94	67	71	64
	189	166	198	202	182	210
	239	244	358	323	318	314
	376	375	431	436	446	456
$^4I_{11/2}$	1947	1961	1988	1979	1991	
	1972	1986	2013	2012	2026	
	2022	2014	2032	2043	2065	
	2041		2109	2140	2082	
	2111	2114	2151	2168	2145	
	2134	2143	2209	2222	2203	
$^4I_{13/2}$	3899		3918		3945	
	3904		3956		3978	
	3961		3999		4019	
	4017		4034		4029	
	4037		4104		4112	
	4112		4173		4153	
	4112		4209		4238	
$^4I_{15/2}$	5846		5819		5892	
	5857		5915		5912	
	5919		5987		5960	
	6054		6031		6047	
	6133		6127		6170	
	6198		6252		6315	
	6199		6392		6334	
	6258		6445		6509	
$^4F_{3/2}$	11 380	11 382	11 404	11 404	11 466	11 477
	11 393	11 401	11 539	11 545	11 574	11 597
$^2H2_{9/2}$ &	12 370	12 390	12 419	12 430	12 490	12 502
$^4F_{5/2}$	12 403	12 408	12 532	12 525	12 545	12 556
	12 456	12 486	12 556	12 595	12 598	12 605
	12 535	12 519	12 605	12 595	12 635	12 639
	12 557		12 630	12 667	12 692	12 682
	12 574	12 599	12 739	12 752	12 731	12 725
	12 656		12 825	12 788	12 830	12 790
	12 678	12 680	12 867		12 881	12 840
$^4F_{7/2}$	13 360	13 336	13 365	13 347	13 452	13 416
$^4S_{3/2}$	13 376		13 470	13 481	13 481	13 527
	13 414	13 409	13 532	13 515	13 545	13 576
	13 443	13 442	13 575	13 579	13 556	13 576
	13 449	13 442	13 589	13 579	13 614	13 635
	13 475	13 465	13 637	13 635	13 674	13 686
$^4F_{9/2}$	14 599	14 592	14 687	14 670	14 752	14 724
	14 608	14 606	14 695	14 716	14 764	14 774
	14 662	14 661	14 757	14 776	14 797	14 812
	14 730	14 721	14 832	14 835	14 902	14 868
	14 750	14 735	14 916	14 905	14 930	14 930

Table 2 *continued*

	Energy level (cm^{-1})					
	$NdVO_4$		$LaVO_4:Nd^{3+}$		$NdPO_4$	
	Calculated	Experimental	Calculated	Experimental	Calculated	Experimental
$^2H2_{11/2}$	15 811	15 787	15 947	15 924	15 975	15 960
	15 820	15 820	15 952	15 924	15 981	15 960
	15 836		15 976	15 961	16 005	15 993
	15 844		15 992	15 989	16 021	16 025
	15 847	15 866	16 012	16 020	16 039	16 049
	15 863	15 966	16 040	16 052	16 053	16 085
$^4G_{5/2}$ &	16 863	16 851	17 038	17 000	17 135	17 099
$^2G1_{7/2}$	16 984	16 996	17 096	17 152	17 211	17 232
	17 049		17 212	17 221	17 324	17 310
	17 171	17 167	17 294	17 290	17 383	17 387
	17 184		17 332	17 329	17 407	17 419
	17 239	17 223	17 380	17 368	17 447	17 454
	17 257	17 267	17 422	17 415	17 487	17 488
$^4G_{7/2}$	18 776		18 908	18 947	19 015	19 045
	18 832	18 819	18 982	18 979	19 076	19 062
	18 875	18 870	19 066	19 043	19 137	19 136
	18 948	18 935	19 112	19 145	19 200	19 225
$^2K_{13/2}$ &	19 151		19 345	19 351	19 448	19 466
$^4G_{9/2}$	19 173		19 393	19 403	19 487	19 513
	19 328	19 302	19 452		19 537	19 553
	19 330	19 336	19 483		19 582	19 587
	19 348		19 507	19 498	19 597	
	19 379	19 369	19 536		19 622	19 614
	19 383		19 563		19 637	19 645
	19 405	19 405	19 588		19 692	19 710
	19 453	19 443	19 626	19 618	19 741	
	19 475		19 653	19 700	19 745	19 766
	19 536		19 815	19 800	19 863	19 854
	19 536		20 032	20 012	20 016	20 043
$^2G1_{9/2}$	20 777		20 898	20 942	20 991	21 025
	20 789	20 814	21 007	20 996	21 064	21 063
	20 870	20 859	21 034	21 018	21 105	21 084
	20 891	20 885	21 046	21 039	21 124	21 114
	20 923	20 959	21 100	21 076	21 138	21 154
$^2D1_{3/2}$	21 022	21 012	21 128	21 139	21 217	21 212
	21 053	21 065	21 209	21 209	21 293	21 278
$^2K_{15/2}$ &	21 171	21 128	21 334	21 323	21 438	21 434
$^4G_{11/2}$	21 184	21 156	21 386	21 363	21 500	21 489
	21 224	21 241	21 450	21 445	21 550	21 550
	21 241	21 272	21 490		21 571	21 570
	21 335	21 351	21 496	21 498	21 636	21 613
	21 370	21 378	21 517		21 645	21 629
	21 410	21 409	21 539		21 683	21 666
	21 429		21 567	21 566	21 692	21 693
	21 457	21 461	21 642	21 629	21 725	21 719
	21 474		21 668	21 668	21 748	21 743
	21 484	21 488	21 701	21 698	21 788	21 780
	21 507		21 741	21 744	21 842	21 817

Table 2 *continued*

	Energy level (cm^{-1})					
	$NdVO_4$		$LaVO_4:Nd^{3+}$		$NdPO_4$	
	Calculated	Experimental	Calculated	Experimental	Calculated	Experimental
	21 550		21 820	21 861	21 880	21 904
	21 591	21 587	22 044	22 012	22 046	22 023
$^2P_{1/2}$	23 074	23 080	23 227	23 229	23 328	23 329
$^2D1_{5/2}$	23 631	23 639	23 685		23 776	23 765
	23 675	23 674	23 880		23 932	23 924
	23 680	23 674	23 974		24 004	24 020
$^2P_{3/2}$	25 987	25 989	26 062		26 170	26 182
	26 011	26 005	26 221		26 306	26 318
$^4D_{3/2}$	27 666	27 671	27 764		28 034	28 046
	27 747	27 736	27 880		28 127	28 128
$^4D_{5/2}$	27 839		27 999		28 243	
	27 872	27 887	28 182		28 317	28 305
	28 061		28 269		28 499	28 514
$^4D_{1/2}$	28 291	28 285	28 568		28 753	28 743
$^2I_{11/2}$	28 735		28 910		29 130	29 113
	28 745		29 091		29 169	
	28 909		29 200		29 359	29 383
	28 978		29 312		29 468	29 450
	29 066		29 444		29 479	
	29 085		29 464		29 539	29 533
$^2L_{15/2}$	29 631		29 697		30 000	29 986
$^4D_{7/2}$	29 638		29 859		30 006	
	29 679		29 881		30 110	
	29 710		29 891		30 137	
	29 743		29 961		20 179	
	29 823		30 064		30 198	
	29 841		30 089		30 293	
	29 880		30 188		30 384	
	29 891					

relatively high B_q^k-values for $YVO_4:Nd^{3+}$ can be explained in a similar way; the Nd^{3+} ion is experiencing a stronger crystal-field effect in replacing a much smaller Y^{3+} matrix cation, reversing the theoretical behaviour. Our values for $NdVO_4:Nd^{3+}$ are usually somewhat smaller than those for $YVO_4:Nd^{3+}$, well in line with the previous reasoning.

3.4. Luminescence spectra of Eu^{3+} in $LaVO_4$ and $LaPO_4$

The emission of the Eu^{3+} ion in both lanthanum matrices originates mainly from the lowest level $^5D_0$ of the ^5D manifold to the different crystal-field levels of the ground multiplet $^7F_{0-4}$. An order-of-magnitude weaker emission could be observed from the higher ^5D levels, $^5D_1$ and $^5D_2$, however. The emission from the excited $^5D_{1-4}$ levels of the Eu^{3+} ion is rather efficiently quenched by multiphonon relaxation of the excitation energy. In the $LaVO_4$ and $LaPO_4$ matrices the lattice phonons of highest energy are

Table 3. Free-ion and crystal-field parameters for the Nd^{3+} ion in $NdVO_4$, $LaVO_4$ and $NdPO_4$. The values in parentheses refer to the estimated standard deviation of the parameter values. The parameter values in square brackets were not varied during the optimization process.

	Value (cm^{-1})		
Parameter	$NdVO_4$	$LaVO_4$	$NdPO_4$
E^0	12 038 (1)	12 144 (1)	12 150 (1)
E^1	4740 (1)	4810 (1)	4804 (1)
E^2	23.15 (2)	23.34 (2)	23.45 (1)
E^3	475.8 (1)	483.5 (1)	484.6 (1)
ζ	869.5 (6)	871.1 (7)	875.2 (6)
α	17.28 (5)	20.39 (5)	20.48 (5)
β	−568 (1)	−646 (1)	−573 (1)
γ	[1500]	[1500]	[1500]
T^2	[330]	241 (5)	[300]
T^3	29.6 (2.4)	36.1 (2.7)	24.0 (2.1)
T^4	111 (3)	99.3 (3.3)	95.0 (2.7)
T^6	−249 (5)	−238 (8)	−274 (6)
T^7	332 (6)	288 (12)	338 (6)
T^8	[330]	197 (13)	329 (11)
B_0^2	−70 (4)	−830 (3)	−655 (14)
B_2^2		213 (4)	104 (15)
B_0^4	280 (9)	−769 (7)	−700 (38)
B_2^4		562 (5)	221 (38)
B_4^4	1138 (3)	383 (6)	693 (25)
B_0^6	−1017 (7)	−798 (9)	−1047 (46)
B_2^6		−702 (6)	811 (34)
B_4^6	88 (7)	−105 (9)	−189 (56)
B_6^6		−563 (7)	−63 (47)
Number of levels	71	74	90
RMS deviation	15	20	17

nearly 900 cm^{-1} which means that at least three phonons are needed to fill the energy gap of 2000 cm^{-1} between the $^5D_1$ and $^5D_0$ (as well as between the $^5D_2$ and $^5D_1$) levels. Such a process involving a simultaneous absorption of three phonons is not highly improbable and thus explains the weak emission from the $^5D_{1-2}$ levels.

As was the case with the absorption spectra of the Nd^{3+} ion also the luminescence spectra of Eu^{3+} contained vibronic side bands (figure 4). However, the $^7F_{0-4}$ energy level scheme could be derived from the emission spectra as nearly complete, i.e. for $LaVO_4$ 24 levels and for $LaPO_4$ 23 out of 25 (table 4). The energy level schemes are very similar and, accordingly the results of the crystal-field simulation were also close (table 5). The simulation, as for the Nd^{3+} ion, also reproduces the experimental energy level schemes well (figure 5). However, it should be pointed out that owing to the large number of crystal-field parameters, there might exist other sets of B_q^k-parameters yielding results of the same quality. On the other hand, the similarity of the Eu^{3+} and Nd^{3+} parameter sets (tables 3 and 5) supports the unique nature of the simulation.

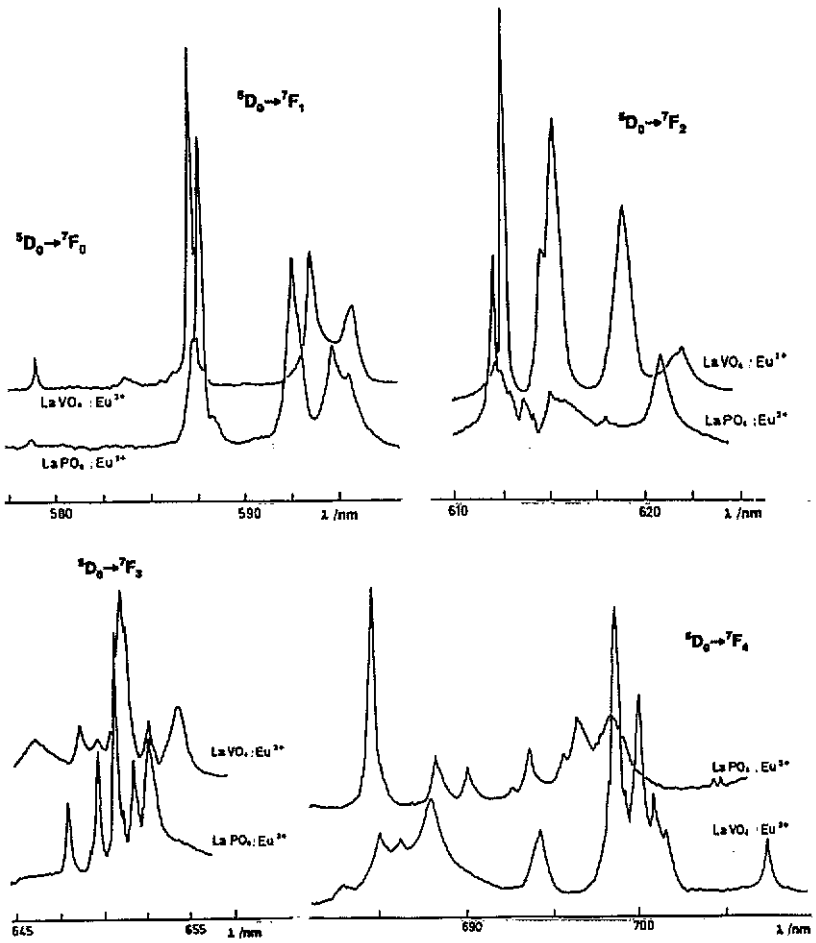

Figure 4. The luminescence spectra of the Eu^{3+} ion in $LaVO_4$ and $LaPO_4$ at liquid-nitrogen temperature.

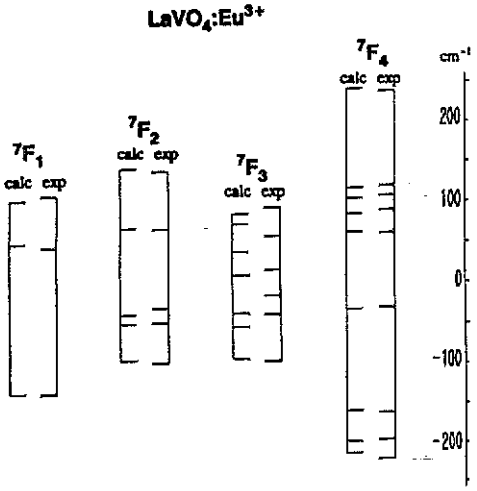

Figure 5. Comparison betweeen the calculated and experimental crystal-field splittings of the $^7F_{0-4}$ energy levels of the Eu^{3+} ion in $LaVO_4$.

Table 4. Experimental and calculated energy levels of the Eu^{3+} ion in $LaVO_4$ and $LaPO_4$.

		Energy level (cm^{-1})			
		$LaVO_4$		$LaPO_4$	
		Experimental	Calculated	Experimental	Calculated
$^7F_0$	A_1	0	0	0	0
$^7F_1$	A_2	240	240	261	262
	B_2	423	428	406	411
	B_1	486	481	464	458
$^7F_2$	B_2	948	952	943	954
	A_1	1000	999		978
	B_1	1018	1010	1021	1019
	A_1	1116	1117	1096	1091
	A_2	1188	1192	1178	1177
$^7F_3$	A_2	1796	1813	1853	1851
	B_2	1857	1855	1881	1859
	B_1	1879	1872	1894	1895
	B_1	1911	1918	1917	1929
	A_2	1953	1948	1927	1936
	B_2	1989	1981	1944	1952
	A_1		1995	1967	1962
$^7F_4$	A_2	2674	2682	2677	2675
	B_1	2699	2697	2755	2751
	A_1	2734	2736	2792	2793
	A_2	2866	2865	2841	2852
	A_1	2958	2960	2863	2868
	B_2	2986	2982	2905	2906
	B_1	3004	3002	2933	2935
	A_1	3016	3015	2963	2955
	B_2	3134	3137		3006
$^5D_0$	A_1	17 271			17 281
$^5D_1$		19 009			
		19 042			
		19 058			
$^5D_2$		21 442			
		21 479			
		21 506			
		21 513			
		21 547			

In contrast with the Nd^{3+} case, there exist ample data for the crystal-field effect of the Eu^{3+} ion in other $REVO_4$ matrices. However, once again it must be concluded that the crystal-field parameter sets for the monazite structure are completely different.

4. Conclusions

The energy level simulations for the Nd^{3+} and Eu^{3+} ions in the $REVO_4$ and $REPO_4$ matrices gave satisfactory results. The B_q^k-parameter sets are very similar for the matrices

Table 5. Crystal-field parameters for $LaVO_4:Eu^{3+}$ and $LaPO_4:Eu^{3+}$. The values in parentheses refer to the estimated standard deviation of the parameter values.

	Value (cm^{-1})	
	$LaVO_4:Eu^{3+}$	$LaPO_4:Eu^{3+}$
B_0^2	−843 (11)	−649 (23)
B_2^2	172 (5)	129 (13)
B_0^4	−928 (15)	−558 (40)
B_2^4	438 (12)	562 (27)
B_4^4	409 (11)	496 (30)
B_0^6	−713 (22)	−512 (61)
B_2^6	−677 (15)	−148 (26)
B_4^6	−568 (12)	−276 (41)
B_6^6	−623 (11)	−318 (33)
RMS deviation	5.4	9

of the same xenotime structure but differ completely from that of the monazite structure. As far as the results for the $NdVO_4$ host are concerned, they are consistent with those published earlier for $YVO_4:Nd^{3+}$ and $YVO_4:RE^{3+}$.

References

[1] Carnall W T, Goodman G L, Rajnak K and Rana R S 1989 *J. Chem. Phys.* **90** 3443
[2] Morrison C A and Leavitt R P 1979 *J. Chem. Phys.* **71** 2366
[3] Caro P, Derouet J, Beaury L, Teste de Sagey G, Chaminade J P, Aride J and Pouchard M 1981 *J. Chem. Phys.* **74** 2698
[4] Jayasankar C K, Richardson F S and Reid M F 1989 *J. Less-Common Met.* **148** 289
[5] Crosswhite H M 1977 *CNRS Coll. 225* p 65
[6] Rajnak K and Couture L 1981 *Chem. Phys.* **55** 331
[7] Nutter P, Weber M and Harrison M 1965 *Raytheon Report* AFML-TR-65-57
[8] Jezowska-Trzebiatowska B, Ryba-Romanowski W, Mazurak Z and Hanuza J 1980 *Chem. Phys.* **50** 209
[9] Schwartz R W, Faulkner T R and Richardson F S 1979 *Mol. Phys.* **38** 1767
[10] Foster D R, Richardson F S and Schwartz R W 1985 *J. Chem. Phys.* **82** 601
[11] da Gama A A S, de Sa G F, Porcher P and Caro P 1981 *J. Chem. Phys.* **75** 2583
[12] Görller-Walrand C, Fluyt L, Porcher P, da Gama A A S, de Sa G F, Carnall W T and Goodman G L 1989 *J. Less-Common Met.* **148** 339
[13] Morrison C A, Wortman D F, Leavitt R P and Jenssen H 1980 *Report* HDL-TR-1897
[14] Barthem R B, Buisson R and Cone R L 1989 *J. Chem. Phys.* **91** 627
[15] Caro P, Derouet J, Beaury L and Soulie E 1979 *J. Chem. Phys.* **70** 2542
[16] Chang N C, Gruber J B, Leavitt R P and Morrison C A 1982 *J. Chem. Phys.* **76** 3877
[17] Beaury L 1988 *PhD Thesis* Universite de Paris-Sud
[18] Antic-Fidancev E, Lemaitre-Blaise M, Beaury T, Teste de Sagey G and Caro P 1980 *J. Chem. Phys.* **73** 4613
[19] Karayianis N, Morrison C A and Wortman D F 1976 *Solid State Commun.* **18** 1299
[20] Morrison C A, Karayianis N and Wortman D F 1977 *Report* HDL-TR-1788 (Harry Diamond Laboratory)
[21] Beaury L and Caro P 1990 *J. Physique* **51** 471
[22] Gruber J B, Leavitt R P and Morrison C A 1983 *J. Chem. Phys.* **79** 1664
[23] Taibi M, Aride J, Antic-Fidancev E, Lemaitre-Blaise M and Porcher P 1989 *Phys. Status Solidi* a **115** 523
[24] Gruber J B, Hills M E, Morrison C A, Turner G A and Kokta M R 1988 *Phys. Rev.* B **37** 8564
[25] Antic-Fidancev E, Jayasankar C K, Lemaitre-Blaise M and Porcher P 1986 *J. Phys. C: Solid State Phys.* **19** 6451

[26] Nekvasil V 1978 *Phys. Status Solidi* b **87** 317
[27] Karayianis N, Morrison C A and Wortman D F 1976 *Report* HDL-TR-1776 (Harry Diamond Laboratory)
[28] Hayhurst T, Shalimoff G, Conway J G, Edelstein N, Boatner L A and Abraham M M 1982 *J. Chem. Phys.* **76** 3960
[29] Karayianis N, Morrison C A and Wortman D F 1975 *J. Chem. Phys.* **62** 4125
[30] Guo M-D, Aldred A T and Chan S-K 1987 *J. Phys. Chem. Solids* **48** 229
[31] Gruber J B and Satten R A 1963 *J. Chem. Phys.* **39** 1455
[32] Kato Y, Nagai T and Saika A 1977 *Bull. Chem. Soc. Japan* **50** 862
[33] May P S, Jayasankar C K and Richardson F S 1989 *Chem. Phys.* **138** 123
[34] Wortman D F, Morrison C A and Karayianis N 1977 *Report* HDL-TR-1794 (Harry Diamond Laboratory)
[35] Singh B P, Sharma K K and Minhas I S 1986 *J. Phys. C: Solid State Phys.* **19** 6655
[36] Minhas I S, Sharma K K and Gruber J B 1973 *Phys. Rev.* B **8** 385
[37] Brecher C, Samelson H, Lempicki A, Riley R and Peters T 1967 *Phys. Rev.* **155** 178
[38] Brecher C, Samelson H, Riley R and Lempicki A 1968 *J. Chem. Phys.* **49** 3303
[39] Grenet G, Kibler M, Linares C, Louat A and Gaume F 1977 *Chem. Phys. Lett.* **51** 160
[40] Linares C, Louat A and Blanchard M 1977 *Struct. Bonding (Berlin)* **33** 179
[41] Gaume F, Linares C, Louat A and Blanchard M 1974 *Proc. 11th Rare Earth Research Conf.* vol 1 (Oak Ridge: US Atomic Energy Commission) p 382
[42] Kuse D 1967 *Z. Phys.* **203** 49
[43] Vishwamittar and Puri S P 1974 *Phys. Rev.* B **9** 4673
[44] Knoll K D 1971 *Phys. Status Solidi* b **45** 553
[45] Wortman D F, Morrison C A and Leavitt R P 1974 *J. Phys. Chem. Solids* **35** 591
[46] Baran E J and Aymonino P J 1971 *Z. Anorg. (Allg.) Chem.* **383** 220
[47] Baran E J, Escobar M E, Fournier L L and Filgueira R R 1981 *Z. Anorg. (Allg.) Chem.* **472** 193
[48] Mullica D F, Sappenfield E L and Boatner L A 1990 *Inorg. Chim. Acta* **174** 155
[49] Beall G W, Boatner L A, Mullica D F and Milligan W O 1981 *J. Inorg. Nucl. Chem.* **43** 101
[50] Antic-Fidancev E, Lemaitre-Blaise M and Caro P 1984 *C. R. Acad. Sci. Paris* II **290** 575
[51] Antic-Fidancev E, Lemaitre-Blaise M, Caro P, Piriou B and Strek W 1985 *Rare Earths Spectroscopy* (Singapore: World Scientific) p 354